Computational Materials Science 154 (2018) 243–250

Contents lists available at ScienceDirect

Computational Materials Science

journal homepage: www.elsevier.com/locate/commatsci

A DFT study of H solubility and diffusion in the Fe-Cr system

P. Bruzzoni[a,b,*,1], R.C. Pasianot[a,b,c,1]

[a] Gerencia Materiales, CAC-CNEA, Avda. Gral. Paz 1499, 1650 San Martín, Argentina
[b] Instituto Sabato, UNSAM/CNEA, Argentina
[c] CONICET, Argentina

ARTICLE INFO

Keywords:
Fe-Cr alloys
Hydrogen diffusion
Hydrogen permeation
Density functional theory

ABSTRACT

Density functional theory (DFT) has been used to study the interaction of H with the Fe-Cr system, in particular $Fe_{15}Cr$. We found that the Cr substitutional atom repeals H; consistently, the H diffusion coefficient is predicted to be reduced in ~13% with respect to the pure Fe matrix. Moreover, a reduction of approximately one order of magnitude in the H permeation coefficient with respect to pure Fe is also predicted; the result agrees well with experimental data for 9–12% Cr steels and Fe-Cr alloys, and is attributed mainly to solubility effects. As a complementary study, the (absolute) diffusion coefficient of H in pure Fe was evaluated, obtaining good agreement with experimental data and revealing sizable quantum effects in the temperature range of measurements. Highly converged DFT calculations, that kept errors at a feasible minimum, played an essential role in all these results.

1. Introduction

9–12 wt% Cr steels have received renewed interest in the last years in view of their potential application as structural materials in Generation IV nuclear reactors and prospective fusion reactors [1]. One of the materials degradation mechanisms to be considered in these steels is hydrogen induced cracking [2]. There is a significant amount of experimental work on the interaction between hydrogen and 9–12 Cr steels. Particularly, the results on hydrogen diffusion show the phenomenon of trapping [3], similar to that found in plain carbon or low alloy steels [4]. Regarding steady-state permeation, steels containing 9–13 wt% Cr present coefficients [5–7] which are *ca.* one order of magnitude lower than those of pure Fe, plain carbon steels and low alloy steels [8]. The main objective of the present work is then to study the permeation coefficient of H in the Fe-Cr system by using *ab initio* techniques, and in particular to understand this significant drop. The permeation coefficient is the product of diffusivity and solubility, cf. [9]. In this context, H diffusion in steels is affected by trapping, though not the steady state, as shown for example in [10]. The underlying picture is a mechanism of diffusion through normal lattice sites and traps acting as H accumulators. Then, the relevant parameter for the prediction of the permeation coefficient is H solubility in a perfect metal lattice, so that *ab initio* techniques should be adequate for this purpose.

A few references are available in the field of *ab initio* theoretical calculations on the Fe-M-H system, with M = alloying element including Chromium [11–13]. However, specific works on the Fe-Cr-H system comparable in detail to some on Fe-H [14] are hardly to be found in the literature. As a first approach to the 9–12 wt% Cr ferritic-martensitic steels we have selected the ordered alloy $Fe_{15}Cr$ (Fe-5.8 wt % Cr), $2 \times 2 \times 2$ bcc unit cells. This system is suitable to *ab initio* studies due to the small number of non-equivalent hydrogen sites to be inspected. Furthermore, the ordered $Fe_{15}Cr$ alloy may be representative of the Fe-Cr system in the atomic fraction interval $0 < x_{Cr} < 0.1$, where the presence of short range ordering (SRO) has been observed, with a minimum SRO parameter of ~ -0.03 for the first two shells [15]. The phenomenon has been ascribed to the opposite magnetism of Fe and Cr atoms, and is also linked with an enhanced Cr solubility at those concentrations [16]. Besides $Fe_{15}CrH$, systems with lower x_{Cr} values are here studied in order to assess effects of x_{Cr} on H stability. In brief, we present results of *ab initio* calculations via Density-Functional Theory (DFT) on the interaction of H with the model systems mentioned above. Also included is Fe-H as a reference system, for comparison with previous results in the literature, and as a test of calculations' accuracy. The paper is organized as follows: in Section 2 the details of the systems and the DFT calculations are reported. In Section 3 the results of the calculations are presented and predictions concerning the hydrogen diffusion and permeation coefficients are made and compared with

* Corresponding author at: Gerencia Materiales, CAC-CNEA, Avda. Gral. Paz 1499, 1650 San Martín, Argentina.
E-mail address: bruzzoni@cnea.gov.ar (P. Bruzzoni).
[1] Both authors P. Bruzzoni and R.C. Pasianot contributed equally.

https://doi.org/10.1016/j.commatsci.2018.07.066
Received 12 April 2018; Received in revised form 25 July 2018; Accepted 31 July 2018
Available online 07 August 2018
0927-0256/

experimental data. The concluding remarks follow next.

2. Details on the systems and the DFT calculations

2.1. Method of calculation

The *ab initio* calculations were carried out by using the Vienna Ab-initio Simulation Package (VASP) [17]. The PAW method for the interaction between potential core and valence electrons, together with the PBE functional for exchange and correlation, were chosen [18]. All calculations were spin-polarized and performed on cubic supercells that contain 8 bcc unit cells: Fe_{16}, $Fe_{16}H$, $Fe_{15}Cr$ and $Fe_{15}CrH$ (M_{16} supercells). Also, cubic supercells containing 27 and 64 bcc unit cells (M_{54} and M_{128} respectively) were studied in order to investigate the effect of the proximity of neighbor H and Cr atoms. The H atom, if present, was initially placed in a geometric tetrahedral or octahedral interstice, as described below. A Gamma-centered k-points grid was used, which is the package default recommendation. The adequate energy cutoff (400 eV) and density of k-points (system dependent) were determined after the convergence study reported in Section 3.1. and described with more detail in the Supplementary Material.

For calculations performed at zero stress, the anisotropy of H placed in a tetrahedral or octahedral site of the bcc lattice causes a slight tetragonal distortion [14]. However, this effect was here disregarded, both in the Fe-H and Fe-Cr-H systems, based mainly on the grounds that, in macroscopic samples, H is distributed randomly among tetrahedral or octahedral sites leading to null overall distortion. Therefore, the relaxation runs allowed changes of ion positions but the cell size was kept constant and the shape cubic. In order to obtain the cell size for minimum energy, individual runs at fixed volume were performed as described later on.

The energy of H in a particular site E is generally referred to that of the most stable site $E^{\dagger}$ of the same system. However, for the Fe-Cr-H system, we also find convenient to use a relative energy E_H where the reference is the tetrahedral site in pure Fe, which previous DFT calculations [14] showed to be the fundamental one. This common reference for Fe-H and Fe-Cr-H is necessary for the comparison of experimental permeation coefficients, as will be shown below. E_H is thus calculated by considering the reaction

$$Fe_n\ H + Fe_{n-m}Cr_m \rightarrow Fe_n + Fe_{n-m}Cr_mH,$$

where from

$$E_H = [E(Fe_n) + E(Fe_{n-m}Cr_mH)] - [E(Fe_nH) + E(Fe_{n-m}Cr_m)], \quad (1)$$

Here n = 16, 54 or 128 according to the size of the supercell, and m = 1 usually; however, the combination n= 128 and m= 8 was also studied. In fact $Fe_{120}Cr_8$, an ensemble of 8 $Fe_{15}Cr$ supercells, is key to extrapolate the results to infinite H dilution. Usually, Fe_nH designates a system in which H is located in a tetrahedral site, whereas for $Fe_{n-m}Cr_mH$ it is located in the site of interest, i.e. T_A, T_B, O_A, O_B, etc. (Fig. 1).

2.2. Hydrogen sites

Besides tetrahedral, the octahedral sites in pure Fe were found neither stable nor transition states. Instead, they are rank-2 saddle points [14], *i.e.* a frequency analysis yielded two imaginary frequencies. However, a previous work by the authors on the Fe-Cr-H system pointed to the possible existence of a stable octahedral site [13]. Then, presently, both tetrahedral and octahedral sites were inspected.

We have identified different geometric tetrahedral (T_A … T_D) and octahedral (O_A … O_E) sites in the bcc $Fe_{15}Cr$ system. The subscript (A, B…) varies according to the distance between H and the Cr atom (Fig. 1).

Some of the sites shown in Fig. 1 are equidistant with Cr atoms of neighbor supercells (acknowledging the periodic boundary conditions).

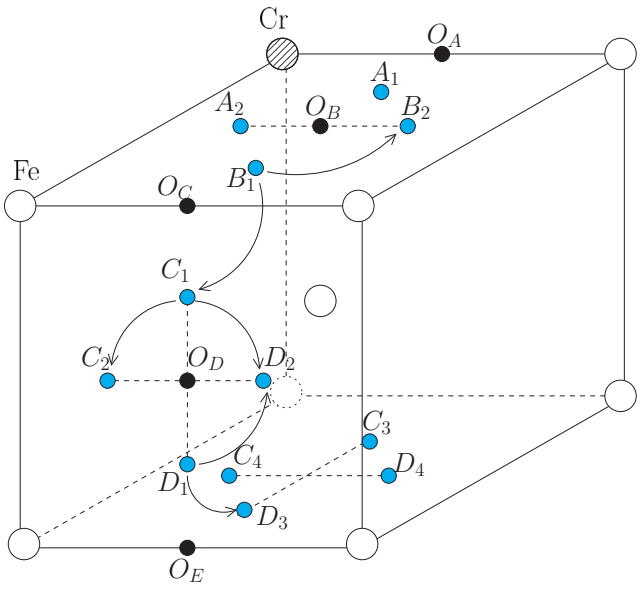

Fig. 1. The different geometric octahedral (O_A, O_B…) and tetrahedral (A, B…) sites identified in the $Fe_{15}Cr$ system. The sites are ordered according to the distance to the Cr atom. The relevant diffusion jumps are also shown.

They can be regarded as "shared" by more than one Cr atom. In this context, O_C, O_D, T_C and T_D are shared by 2 Cr atoms while O_E is shared by 4 Cr atoms.

2.3. Relaxation of the stable sites

The relaxation of the geometrical sites to a more stable configuration was carried out using a quasi-Newton procedure. Only changes of ion positions were allowed, while the cell was kept cubic and at fixed volume. Typically, the relaxation procedure was carried out for at least 12 different cell sizes L (edge length of the supercell) around ± 0.4% of the minimum energy size. The minimum Energy (E_{min}) and respective size (L_{min}) were obtained from a parabolic fit. Each relaxation procedure, carried out by allowing fractional electronic occupancies (Fermi smearing, σ = 0.2 eV), ended with a self-consistent field cycle where Blöchl's methodology for Brillouin zone integrations [19] was applied.

2.4. Frequency analysis and energy barriers

Frequency analysis was performed in order to check whether every relaxed site was indeed stable, as well as to assess jump rates and quantum effects. In [14] it was proposed that the H and Fe vibrations may be decoupled in view of their different masses. In the present work a similar assumption is made though errors were estimated in Section 3.3.

The transition states for the jumps between adjacent stable sites were investigated with the purpose to study the diffusion of hydrogen. The Nudged Elastic Band (NEB) was the standard tool. In selected cases, the NEB results were validated and refined with the Dimer method. The information obtained from the $M_{16}H$ systems (*i.e.* atomic positions) was used to study selected transition states of the larger supercells $Fe_{128}H$ and $Fe_{120}Cr_8H$ *via* the Dimer method.

Regarding quantum effects, these include the zero point energy correction (ZPE) to the stable states, and contributions to the jump rates (tunneling in particular). The former amounts to $\frac{1}{2}h\sum_i \gamma_i$, *i.e.*, a sum over the H real frequencies γ_i (h is the Plancks constant). Frequencies of the M_{16} systems were also used for the M_{128} systems.

2.5. Elastic corrections

As already mentioned, experimental H atomic fractions in samples of Fe and Fe-Cr alloys are usually in the range 10^{-6}–10^{-4}, namely, several orders of magnitude lower than the presently simulated 1:16 to 1:128. Therefore, spurious image interactions introduced by the periodic boundary conditions (PBC) are likely, at least for the smaller cells, and need be accounted for in order to mimic the infinite dilution limit. To this effect, the H atom inserted in a stress-free cell, may be conceived as an elastic dipole (or inclusion) surrounded by a continuous medium. The ensuing rise in stress determines the dipole value, and standard elastic theory allows one to compute the interaction energy with images (to be subtracted). The actual calculations were carried out with the tools provided in [20], including the amendments developed in [21].

A further benefit of the approach is that energies of systems with and without H are compared for fixed volume and shape cells. This avoids possible drawbacks stemming from plane wave basis changes, associated with volume changes, that render less than reliable the corresponding energy difference, aspect especially relevant to our current demands of high accuracy.

3. Results and discussion

3.1. Convergence errors

Energy differences of different H sites in Fe-H systems are typically in the range of some tens of meV. Therefore, in order to obtain sufficiently precise results, a convergence test aimed at obtaining a precision objective of 1 meV was performed on the M_{16} systems, *i.e.* Fe_{16}, $Fe_{16}H$, $Fe_{15}Cr$ and $Fe_{15}CrH$. Details are reported as Supplementary Material.

The results indicate that E_{cutoff} = 400 eV is enough for the required precision objective and was adopted for all calculations. Concerning the density of k-points, the precise calculation of Eq. (1) requires a k-points grid of 8 × 8 × 8 for M_{16} systems. An identical density of k-points is used for the critical (Section 3.9) calculation of Eq. (1) for the T_C site of the $Fe_{120}Cr_8H$ system, namely a 4 × 4 × 4 grid. All the remaining H energies in the $Fe_{120}Cr_8H$ system were calculated as relative to the T_C-site with a 3 × 3 × 3 grid. The relaxations in $M_{16}H$, $M_{54}H$ and other $M_{128}H$ systems were performed with grids of 7 × 7 × 7, 5 × 5 × 5 and 3 × 3 × 3 respectively. The latter grids were also used for the NEB and Dimer calculations. Frequency calculations, computationally expensive, were performed on the $M_{16}H$ systems with a 5 × 5 × 5 grid.

3.2. Search for stable hydrogen sites

After the introduction of H in the potentially stable sites of $Fe_{15}CrH$, and ensuing relaxation, the Cr-H distance was analyzed. It was found that the relaxed Cr-H distance (r) is larger than the original geometrical distance (r_{geom}). This effect is stronger for smaller r values. T_C turned to be the lowest energy site; therefore taken as energy reference. Table 1 reports the geometrical and relaxed Cr-H distances for the different H sites studied and their (relative) energy. All reported energies were calculated as the difference between E vs. L fitting curves taken at the optimal size of the H-free cells.

Table 1 shows that two different relaxed structures originate from the initial octahedral site $O_{B,geom}$: the O_B which is close to the latter, and a further displaced O_B^* both lying on the same cube face as $O_{B,geom}$. The existence of the O_B^* site has been reported in [13]. Table 1 also reports our data for the $Fe_{16}H$ system, where the stable site is tetrahedral (T) with values in good agreement with [14].

As shown below the current O_B^* site is in fact a transition state that links adjacent T_B sites. This is at variance with our previous finding in [13], where O_B was obtained as a local minimum (− 0.94 eV below T_B). However, the current calculations, based on the PAW approach and expansions in terms of plane waves, should be considered more reliable than our former ones [13], based on NC-pseudopotentials and atomic-like (NAO) basis functions (Siesta package).

Table 1
Relaxed H sites in the $Fe_{16}H$ and $Fe_{15}CrH$ systems. r_{geom} = H-Cr distance in the initial (geometrical) site; r = H-Cr distance after relaxation; a = bcc lattice parameter; $E-E^{\dagger}$ and E_H (meV) as explained in the main text. (*) ZPE corrected values.

Site type and system	Site	r_{geom}/a	r/a	$E-E^{\dagger}$	E_H, Eq. (1)
Octahedral, $Fe_{16}H$	O	–	–	175	
Tetrahedral, $Fe_{16}H$	T	–	–	0	
Octahedral, $Fe_{15}CrH$	O_A	0.500	0.575	397	
	O_B	0.707	0.679	235	
	O_B^*	0.707	0.863	143	
	O_C	1.118	1.121	194	
	O_D	1.225	1.235	163	
	O_E	1.500	1.499	195	
Tetrahedral, $Fe_{15}CrH$	T_A	0.559	0.625	144/146*	
	T_B	0.901	0.914	31/31*	
	T_C	1.146	1.150	0	17/16*
	T_D	1.346	1.345	13/13*	

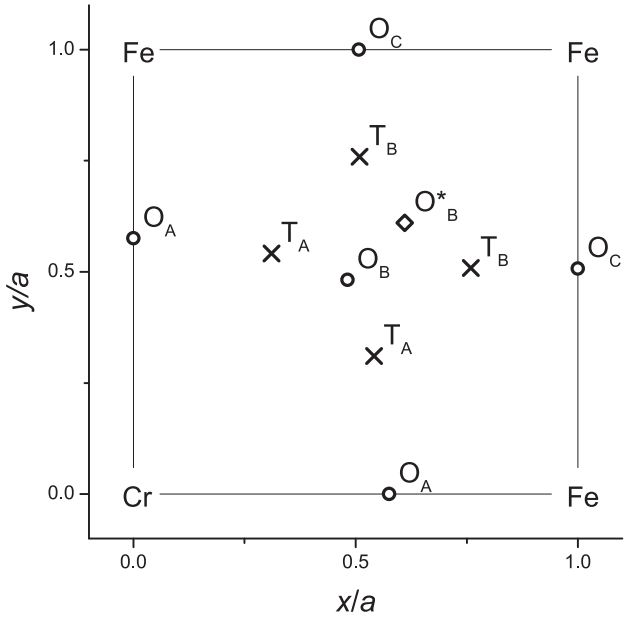

Fig. 2. Positions of the H sites in a (1 0 0) plane in the vicinity of the Cr atom (see also Fig. 1). System: $Fe_{15}CrH$, relaxed; a is the lattice parameter.

After relaxation the tetrahedral sites remained close to the original geometrical position and the only remarkable effect was a displacement away from the Cr atom, as shown in Fig. 2, which depicts atomic positions on the cube face. The energy of T sites is lower than for O sites, but for T_A with respect to O_B^*, which however brings no consequence. Such a relative stability is consistent with previous findings in pure bcc Fe [14,22]. O_B and O_B^* sites appear as bridges between neighbor T_A and T_B respectively. Their (lack of) stability, however, was tested in the following via frequency analysis; in any case O sites may play an important role for H diffusion.

The results indicate that a positive energy is needed to transfer a H atom in a normal interstitial site of bcc Fe to a position near the Cr atom. The substitutional Cr atom can thus be regarded as a “repeller”, *i.e.* the opposite of a trap.

3.3. Frequency analysis on the possible stable sites

The decoupling assumption between H and metal vibrations was checked on the $Fe_{15}Cr$ system by performing two types of runs: (1) Only the H atom is moved; (2) H and also first neighbor metal atoms are

moved, namely, 4 in the case of the T-site and 6 in the case of the O-site. The comparison between (1) and (2) led to estimated errors in the ZPE correction of ~1 meV, which is in line with our precision goal; therefore method (1) was adopted.

Detailed numerical values are reported in Table S1 of the Supplementary Material. All tetrahedral sites possess three vibration modes with real frequencies; they are indeed stable sites. The near-geometrical sites O_A…O_E exhibit two modes with imaginary frequencies, therefore they are rank 2 saddles. The special $O_B{}^*$ site shows only one mode with imaginary frequency, indicative of a transition state. It bridges the jump between neighbor T_B sites (confirmed *via* NEB analysis).

These results are in agreement with the findings of Jiang and Carter for Fe [14] and show that the characteristics of the H sites in the $Fe_{15}Cr$ system are similar to those in pure iron.

Regarding the (relative) ZPE corrections, they are all in the order of 1 meV as already reported in Table 1.

3.4. Effect of Cr concentration on H energy

Due to periodicity restrictions, the $Fe_{15}CrH$ supercell allows to study only four different tetrahedral sites and five different octahedral ones. The fact that the system is periodic implies that Cr atoms in adjacent supercells influence the H atom. In view of this effect larger supercells (*i.e.* $Fe_{53}CrH$ and $Fe_{127}CrH$) were studied with the purpose of minimizing the contribution of the extra Cr atoms on the H energy at a particular site. Although these ordered systems do not exactly represent (partially or totally disordered) real steels, they may show the trend regarding the dependence of H energy on x_{Cr}.

The energies of the different sites T_A … T_D, and O_A … O_E for the different supercells $Fe_{15}CrH$, $Fe_{53}CrH$ and $Fe_{127}CrH$ are reported in Table 2, where the reference energy is that of the tetrahedral site of pure iron, Eq. (1). This helps visualizing the effect of replacing Fe by Cr in the metallic lattice. The frequency data of the $Fe_{15}Cr$ and Fe_{16} systems were used for the ZPE corrections.

The transition from $Fe_{15}CrH$ to $Fe_{53}CrH$ and finally to $Fe_{127}CrH$ can be viewed as pulling out second neighbor Cr atoms from the H atom placed in the T_A…T_D sites. The general trend is a reduction of H energy as n increases. This decrease amounts, globally, ~15 mV for T_A…T_C and ~30 mV for T_D. It is worth noting that the energy of the T_C and T_D sites in the largest system (*i.e.* $Fe_{127}CrH$) is very close to that of the T site in pure iron. It appears that the influence of an isolated Cr atom immersed in a Fe matrix does not extend beyond ~1.2 times de bcc cell parameter. The repelling behavior of the TA site is a common feature of many alloying elements including Cr, as already reported [11,12] for M_{54} cells using VASP and Wien2K codes respectively. The peculiar result for Cr and a few others is that the repulsive effect extends to higher order shells. Present findings are in agreement with [11] and [12], except that for the latter the third and fourth shells become attractive. From a technical point of view, $Fe_{53}Cr$ roughly resembles low-chromium steels such as SAE 4140 low alloy steel and ASTM A588 high-strength low-alloy steel, while $Fe_{15}Cr$ approximately describes ferritic-martensitic 9–12%Cr steels. The $Fe_{53}Cr$ supercell contains a total of 324 T sites, and only 12 out of these are T_A or T_B, thus amounting to a fraction of 1:27 high-energy T sites. The qualitative prediction is that most H sites in low-chromium steels are similar to the H sites in pure iron, while most H sites in ferritic-martensitic 9–12% Cr steels are substantially different from the sites in pure iron. It must be noted that these considerations refer to defect-free materials, to make the difference with trap sites associated with defects.

Table 2
H Energy (E_H) in the different stable sites of the $Fe_{n-1}CrH$ systems (n = 16, 54 and 128). Reference is T site in Fe_nH.

Site	E_H (meV), DFT/ZPE corrected*.		
	$Fe_{15}CrH$	$Fe_{53}CrH$	$Fe_{127}CrH$
T_A	161/161*	163/164*	145/146*
T_B	48/47*	40/39*	36/35*
T_C	17/16*	11/10*	−1/−2*
T_D	30/28*	8/6*	5/3*

Table 3
Energies of the stable sites (including ZPE corrections*) and transition states for pure Fe and $Fe_{15}Cr$. (†) indicates reference site. Notice the different cell sizes (M_{16} and M_{128}) in the last columns.

System	Reference (†)	Site/TS	$E-E^\dagger$	
			H:Me = 1:16	H:Me = 1:128
Fe_{16}	T	T-T	106	89
$Fe_{15}Cr$	C	A	144/146*	138/140*
		B	31/31*	24/24.0*
		D	13/13*	23/23*
		B–B	134	122
		B–C	119	101
		C–C	95	83
		C–D	102	90
		D_1–D_2	118	106
		D_1–D_3	133	119
	T	C	17/16*	16/15*

3.5. Transition states

The Fe_{16} system presents only one possible H jump between neighbor stable sites: the T-T jump. Contrarily, in the $Fe_{15}Cr$ system there is a variety of them. Since all stable sites in $Fe_{15}Cr$ are tetrahedral, the notation is from now simplified by using A, B, C, D instead of T_A, T_B, T_C, T_D. Site A was discarded on the grounds of its high energy and further instabilities that appeared in the frequency analysis.

As mentioned earlier, the structure of the transition state (TS) was determined on the M_{16} systems *via* the NEB method with 7 intermediate (linearly interpolated) images between the stable sites, and later refined with the Dimer method. The different jumps in $Fe_{15}Cr$, Fig. 1, are reported in Table 3 together with the calculated TS energies.

Details on the TS frequencies are provided in Table S2 of the Supplementary Material; not unexpectedly they are all very similar to the Fe_{16} T-T case (values in THz): $\nu_1 = 58.3$; $\nu_2 = 36.3$; $\nu_3 = 20.4$ (imaginary).

With the aim of predicting the H diffusion coefficient, Table 3 reveals significant differences between M_{16} and M_{128} systems. Therefore, H-H interaction effects need to be tested and subtracted in order to attain the infinite dilution limit. Moreover, quantum effects may involve not only a mere ZPE correction but also tunneling. We consider the first issue next, while the second one is treated in the following section.

We performed simulations using M_{16} and M_{128} cells while in parallel, applied elastic corrections as outlined in Section 2.5. As expected, the latter became smaller with cell size, turning negligible for M_{128}, meaning that infinite dilution was indeed reached. Therefore energies from the latter size were used in the actual calculations.

In this context, we found that corrected energies for $Fe_{16}H$ cells matched results of $Fe_{128}H$ simulations with high precision; *e.g.* the T-T barriers were 90 and 89.3 meV respectively.

Unfortunately, corrections for $Fe_{15}CrH$ with respect to $Fe_{120}Cr_8H$ fell outside our precision goal, meaning that (costlier) simulations with the latter cell size were really necessary. The reasons behind the discrepancy are unclear; we speculate they might be related to a less homogeneous (equivalent) medium of the Cr-containing cells as compared with the pure Fe ones.

3.6. The hydrogen diffusion coefficient. Calculation method

From the calculated barriers and frequencies it is possible to predict the H diffusion coefficient D. For this purpose we deviated from the approach followed in [14]. These authors used the semiclassical transition state theory as developed by Kehr [23] and arrived to an expression with a pre-exponential factor that depends linearly on T and a ZPE-corrected energy barrier, Eq. (3) of [14]:

$$D = \frac{2}{3}x^2 k, \quad \text{with} \quad k = \frac{k_B T}{h}\exp\left(-\frac{\Delta E_{ZPE}}{k_B T}\right), \tag{2}$$

where x is the jump length. The pre-exponential factor in Eq. (2) does not depend on the vibration frequencies; then, it appears to be a limiting expression for low temperature, cf. [24]. Instead, we followed a more general approach proposed by Fermann and Auerbach [25], where the rate constant is given by their Eq. (2.12),

$$k = \frac{k_B T}{h}\cdot\frac{Q^{\ddagger}}{Q^{r}}\cdot\Gamma(T). \tag{3}$$

Above, $Q^{\ddagger}$ is the total vibrational partition function at the transition state and Q^{r} is the same for the reactants. $\Gamma(T)$ is a correction factor that accounts for quantum tunneling. Eq. (3) can be further elaborated [24]:

$$\frac{k_B T}{h}\cdot\frac{Q^{\ddagger}}{Q^{r}} = \frac{\prod_{i=1}^{N} f(h\nu_i/2k_B T)}{\prod_{j=1}^{N-1} f(h\nu_j^{\dagger}/2k_B T)}\frac{\nu_1 \times \nu_2 \times \cdots \times \nu_N}{\nu_1^{\dagger} \times \cdots \times \nu_{N-1}^{\dagger}}\exp\left(-\frac{\Delta E}{k_B T}\right), \tag{4}$$

Here, $f(x) = \sinh x/x$, ν_i and $\nu_j^{\dagger}$ are the normal mode real frequencies of the stable state and transition state respectively, and ΔE is the (standard) energy barrier. At very high temperature $f(x) \to 1$ and Eq. (4) tends to the classical Vineyard's expression [26] without quantum effects.

Concerning the $\Gamma(T)$ factor, an approximate expression valid when $h|\nu_N^{\dagger}|/k_B T < 2\pi$ is given by Eq. (2.13) of [25]:

$$\Gamma(T) = \frac{h|\nu_N^{\dagger}|/2k_B T}{\sin(h|\nu_N^{\dagger}|/2k_B T)}. \tag{5}$$

3.7. Diffusion coefficient in pure Fe

First, the diffusion coefficient of hydrogen in pure iron was predicted. The necessary data is contained in Table 3 and Tables S1–S2 of the Supplementary Material. The distance between two adjacent geometrical T sites is $\frac{\sqrt{2}}{4}a$, *i.e.* ~1.00 Å, and the energy barrier is 89.3 meV (Table 3). The critical value of T that makes $h|\nu_N^{\dagger}|/k_B T = 2\pi$ is 156 K, well below the range 270 K ≤ T ≤ 800 K where these calculations are intended to be compared with experimental data; therefore Eq. (5) was used.

Fig. 3 shows the predicted diffusion coefficient, together with selected experimental values. It is important to select experiments in which surface effects are minimized to ensure volume control, and trapping is reduced through careful annealing and use of high purity material. The works of Quick and Johnson [27] and Riecke and Bohnenkamp [10] meet these requirements. The calculated values of the diffusion coefficient depart from the classical straight line. Quantum effects, namely ZPE correction and tunneling, are important and account for an increase of D by a factor of *ca.* 2 with respect to the classical limit at room temperature. The apparent activation energy, taken from the slope of the Arrhenius plot, gradually decreases as the temperature decreases. For example, at room temperature the apparent activation energy is ~43 meV instead of the calculated energy barrier of 89.3 meV which is the high temperature limit. The former value is even slightly lower than the ZPE-corrected energy barrier (46 meV).

Also shown is the approach *via* Eq. (2). It turns out that the quantum correction is lower in this case, which may be attributed to the fact that quantum tunneling is not considered. Besides, since Eq. (2) is a low temperature approximation, it does not tend to the classical limit at high temperatures.

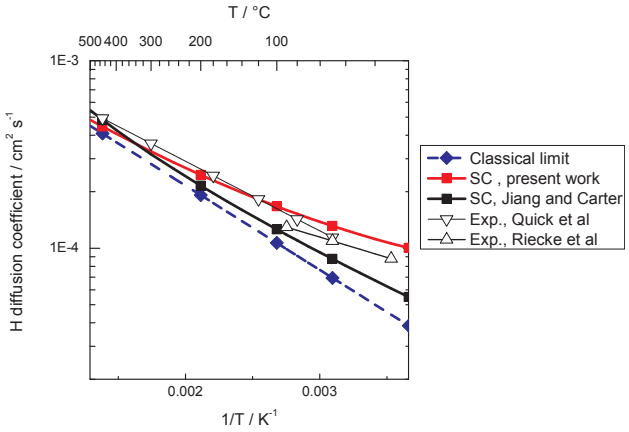

Fig. 3. Diffusion coefficient of H in iron. Experimental values from literature and present calculations. SC stands for "semiclassical transition state theory". Open / filled symbols are experimental/calculated values.

The experimental values of the diffusion coefficient at room and high temperature are in close agreement with the calculations. The decreasing trend of the experimental activation energy with decreasing temperature is adequately reflected by our approach. Moreover, the theoretical pre-exponential factor fits well the experimental data. This shows the importance of quantum effects in the present system.

3.8. Diffusion coefficient in $Fe_{15}Cr$

The task to predict the diffusion coefficient of H in the ordered alloy is $Fe_{15}Cr$ is more complex. The difficulty arises from the multiple jumps, as reported in Table 3 and shown in Fig. 1. In order to develop a simple model, the following assumptions were made:

(i) Only tetrahedral sites and jumps between them are considered. This is justified by the high energy of the octahedral sites (Table 2), and their instability (rank 2 saddles).
(ii) The Cr atom originates an "exclusion zone" for H, which is constituted by the nearest tetrahedral sites, *i.e.* the T_A. This is justified by their high energy (Table 1).
(iii) The small differences in lattice geometry between $Fe_{15}Cr$ and pure Fe, as well as the respective H frequencies, are neglected.

In fact we focused on the ratio of the diffusion coefficients in the two media, $f_D = D/D_{Fe}$. With the above assumptions, this amounts to consider scaled jump frequencies of the $Fe_{15}Cr$ system referred to pure Fe, namely,

$$W_i = \exp\left(\frac{E_m^i - E_m^0}{k_B T}\right), \tag{6}$$

where E_m^i is a migration barrier for $Fe_{15}Cr$, and E_m^0 is the same for pure Fe. Notice that even if quantum effects matter, the above holds, cf. Eqs. (4) and (5), as long as assumption (iii) is valid.

Thus we set up a kinetic Monte Carlo approach taking B, C, and D as equilibrium sites, together with possible jumps BB, CC, D_1D_2, D_1D_3, BC and CD (Fig. 1). The simulation supercell consisted of 5 × 5 × 5 unit cells of $Fe_{15}Cr$ repeated periodically; a H atom was then placed at any of the equilibrium sites according to their statistical weight, and forced to walk n steps through the lattice (history). The clock was advanced at every step by $\Delta t = 1/\sum W_i$, adding to a total of t_n at history end. A partial, dimensionless, diffusion coefficient was then computed as a

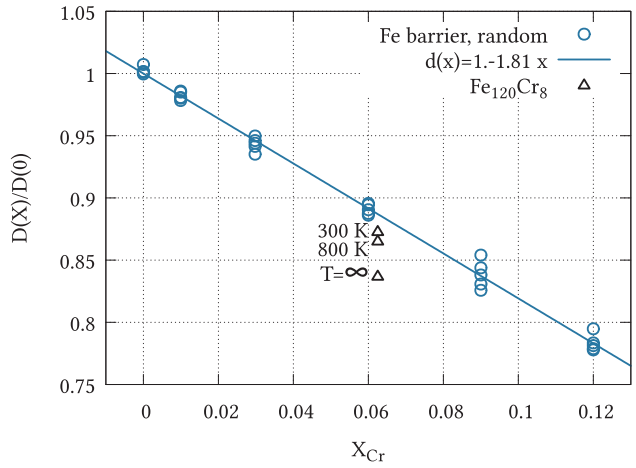

Fig. 4. Estimation of the H diffusion coefficient ratio f_D = D(X)/D(0) in Fe-Cr alloys by a random walk virtual experiment; see main text for details.

mean square deviation over the history,

$$d = \frac{\langle z^2\rangle_n - \langle z_n\rangle^2}{a^2 t_n}, \tag{7}$$

where z refers to a Cartesian coordinate. The process was repeated N times, and finally the ratio f_D obtained by averaging,

$$f_D = \frac{\langle d\rangle_N}{d_0}; \tag{8}$$

Here $d_0 = 0.083$ is the same as $\langle d\rangle_N$, but performed over the pure Fe lattice and using unit jump frequencies, $W_i = 1$. Typical values n and N were 20 and 10,000 respectively, that assure convergence of f_D to better than 1%.

Fig. 4 shows our calculated values of f_D for three temperatures, 300 K, 800 K, and $T \to \infty$. The relatively narrow spread of the three points and their closeness to the random alloy model (see later on), suggest that the main effect of dissolved Cr upon H diffusion is the blocking of A sites.

The direct comparison of calculated values of D in $Fe_{15}Cr$ with experimental values of alloys with similar composition is not pertinent, since the presence of H traps associated with defects is likely in Fe-Cr alloys. The presence of traps leads to the fact that experimental D values show a high scatter and lie below the calculated one.

In order to put the above results in a wider perspective, we also studied the f_D ratio for random Fe-Cr alloys, by fixing the barriers to that of pure Fe, though still keeping nearest neighbors (T_A) sites of Cr atoms blocked. The result is shown by the fitted straight line in Fig. 4; as expected f_D decreases with Cr content. In particular, for the concentration appropriate to $Fe_{15}Cr$, the result is a little above of the one for the ordered alloy, consistent with the fact that the latter possesses a larger fraction of tetrahedral sites blocked. It is also interesting to note that the fitting slope, 1.81, is close to 2.0, which is roughly expected from a naive site counting argument, i.e. the number of blocked T-sites per Cr atom (12) to the number of T-sites per lattice node (6).

3.9. Permeation coefficient of H in $Fe_{15}CrH$

It has been mentioned above that the 9–12 wt% Cr steels and Fe-~10 wt% Cr alloys present a permeation coefficient [5,28–33] approximately one order of magnitude lower than that of pure iron [8]. Also, we have modeled the $Fe_{15}Cr$ system as an "ordered" Fe-5.8 wt% Cr alloy. In a steel, the permeation coefficient Φ is a material-dependent parameter that determines the steady-state hydrogen flux $J\,[\frac{molH}{cm^2 s}]$ across a membrane of thickness δ with an input surface in contact with a partial hydrogen pressure p [8]:

$$J = \Phi\frac{\sqrt{p}}{\delta}.$$

Indeed, the permeation coefficient is the product of the diffusion coefficient D and the *S*ieverts constant S [9]. In the classical frame:

$$D = D_0 \exp(-E_D/k_B T)$$

,

$$S = S_0 \exp(-E_s/k_B T)$$

,

$$\Phi = \Phi_0 \exp(-(E_D + E_s)/k_B T).$$

E_D is the energy barrier for diffusion and E_s is the energy of the stable site relative to a definite reference, *i.e.* H_2 (g) at $p = 1$ bar. Theoretical calculations of E_D and E_s were given here as energy barriers and energies of stable sites. E_s is in fact the energy of the site referred to the energy of molecular hydrogen, but for the present discussion the latter value is just a constant that cancels out. The ratio of the H permeation coefficients in the $Fe_{15}Cr$ system relative to Fe_{16}, neglecting (eventually) quantum effects is then:

$$f_\Phi = \frac{\Phi_{Fe15Cr}}{\Phi_{Fe16}} = f_S f_D, \tag{9}$$

$$f_S = \frac{S_0(Fe_{15}Cr)}{S_0(Fe_{16})} exp\left(\frac{-[E_S(Fe_{15}Cr) - E_S(Fe_{16})]}{k_B T}\right), \tag{10}$$

$$f_D = \frac{D_0(Fe_{15}Cr)}{D_0(Fe_{16})} exp\left(\frac{-[E_D(Fe_{15}Cr) - E_D(Fe_{16})]}{k_B T}\right). \tag{11}$$

Eqs. (9)(11) show that f_Φ is the result of two contributions:

(i) A ratio of Sieverts constants f_S that is related to the relative energy of H in the stable sites of $Fe_{15}Cr$ referred to the stable site of Fe_{16}.
(ii) A ratio of diffusion coefficients f_D.

Strictly, Eqs. (10) and (11) apply to systems with only one stable site, not necessarily to the present case with multiple stable sites, that needs a particular analysis. Such analysis has been made in Section 3.8 for f_D, where we have shown that it is about unity and changes very little with temperature. Regarding f_S, it may be calculated as hinted in Eq. (10) above. The four sites A…D have equal number densities; then, the ratio of the Sieverts constants is expressed as:

$$f_S = \frac{e^{-\frac{E_{H,A}}{k_B T}} + e^{-\frac{E_{H,B}}{k_B T}} + e^{-\frac{E_{H,C}}{k_B T}} + e^{-\frac{E_{H,D}}{k_B T}}}{4}, \tag{12}$$

where $E_{H,i}$ (i = A, B, C, D) is the energy of H at an i -site of the $Fe_{120}Cr_8$ system referred to the energy of H in the T-site of Fe_{128} system. In fact, the term corresponding to the A site was discarded because it is negligible or considered as not stable, Section 3.5. Eq. (12) is rearranged in the following way:

$$f_S = \frac{e^{-\frac{E_{H,C}}{k_B T}}\left(e^{-\frac{\Delta E_B}{k_B T}} + 1 + e^{-\frac{\Delta E_D}{k_B T}}\right)}{4}, \tag{13}$$

where ΔE_B and ΔE_D are the energy levels of the B and D sites referred to the C site in $Fe_{120}Cr_8H$, cf Table 3. The critical calculation of $E_{H,C}$ was performed with a high density of k-points as reported in Section 3.1. The positive value of $E_{H,C}$ means that a lower H solubility in $Fe_{15}Cr$ with respect to pure Fe is predicted. This Sieverts constant ratio has an upper limit of 0.75 at high temperature. To a fair precision, quantum effects are considered here by introducing the pertinent ZPE-corrections. Indeed, the remaining contributions from the quantum oscillators have negligible impact on the solubility ratio. The permeation coefficient ratio was then calculated as $f_\Phi = f_S f_D$ and plotted in Fig. 5 that also shows experimental values for Fe-Cr alloys and commercial Fe-Cr ferritic-martensitic steels [8,28–33]. The atomic fraction of Cr in these

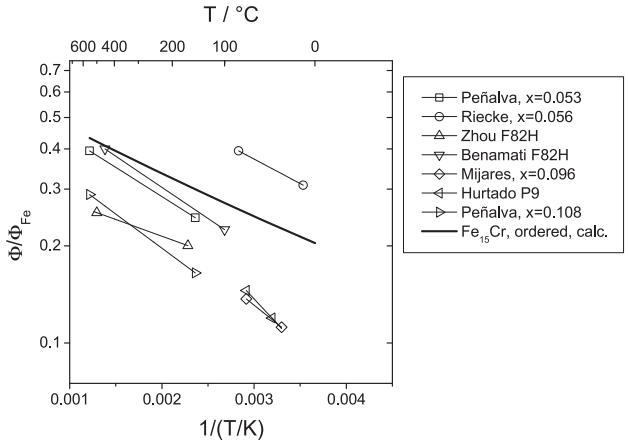

Fig. 5. Permeation coefficient of H in Fe-Cr alloys (x = atomic traction of Cr) and Fe-Cr ferritic-martensitic steels referred to that of pure iron. Steels F82H and P9 are approximately $Fe_{90.9}$ $Cr_{8.4}$ $W_{0.6}$ and $Fe_{89.8}$ $Cr_{9.6}$ $Mo_{0.6}$ respectively. The solid line is the calculated Φ/Φ_{Fe} ratio for the $Fe_{15}Cr$ ordered system.

materials does not necessarily agree with the one of our system, *i.e.* $x_{Cr} = 0.625$. Moreover, the comparison between the present ordered alloy and microscopically disordered materials is not rigorous. As stated in Section 3.8, the Cr atoms are more effective to obstruct the diffusion when placed at ordered positions leading to a slightly lower diffusion coefficient.

It is clear that the factors f_S and f_D are expected to decrease as the x_{Cr} increases. Concerning f_D, the density of forbidden "A" sites increases and the diffusion process is more difficult. Concerning f_S, both the increased density of "A" sites and the expected increase of H energy in the remaining stable tetrahedral sites will cause a reduction of the solubility. This explains, with some exceptions, the position of the experimental data above or below the calculated f_Φ. Regarding the experimental data itself, the Cr content of Benamati et al. samples ($x_{Cr} = 0.084$) [28] is close to ours for $Fe_{15}Cr$ ($x_{Cr} = 0.0625$). In this case the difference in Cr concentration may be compensated by the fact that f_D is lower in the ordered alloy. These authors [28] took measures to avoid oxide formation during their high temperature experiments in vacuum which reduces the H permeation rate. This may be the source of the difference between their data and that of Zhou et al. [29]. Also, the high temperature data of Peñalva et al., $x_{Cr} = 0.052$, [30] appears lower than the low temperature data of Riecke et al., $x_{Cr} = 0.056$, who used an electroplated Pd film to make surface effects negligible [33].

The predicted values of f_Φ are clearly lower than 1 in agreement with experimental data. In fact, the agreement is very satisfactory showing the adequacy of DFT when careful measures to ensure convergence in the range of 1 meV are taken. Since f_D is close to unity, the observed reduction in the permeation coefficient in Fe-Cr systems with respect to pure iron is mainly related to f_S, i.e. solubility effects.

The present solubility results are in apparent contradiction with experiments by Schwarz and Zitter performed on ARMCO iron with different alloying elements [34], that show increased solubility with Cr content. However, Coldwell & McLellan [35] used ad-hoc Fe-Cr alloys prepared from pure metals, and reported negative solution enthalpies which increase in magnitude towards the Fe-rich end, implying a concomitant solubility increase. We speculate that this contradiction between experimental findings might be explained by trapping. As pointed out in the introduction, what really matters for the prediction of the f_Φ ratio is the solubility in the perfect lattice.

4. Conclusions

DFT energy calculations with precision in the order of 1 meV have been performed on Fe and Fe-Cr systems, with the purpose to understand the behavior of H in Fe-Cr alloys and particularly in $Fe_{15}Cr$.

As in pure Fe, stable H sites in $Fe_{15}Cr$ are the tetrahedral interstices.

The H energy in the tetrahedral sites of $Fe_{15}Cr$ decreases as the distance from the Cr atom increases. Substitutional Cr act as a repeller for H. The Cr-first neighbor tetrahedral sites present a markedly higher H energy. Their contribution to the solubility is considered negligible and it is proposed that those sites do not take part in the diffusion process.

The energy barriers for the diffusion of H in $Fe_{15}Cr$ are similar to that of pure Fe.

The elastic model predicts negligible H-H image interactions for the M_{128} cells and correctly extrapolates to infinite dilution $Fe_{16}H$ but not so accurately for $Fe_{15}CrH$.

An approach for the prediction of the H diffusion coefficient in bcc metals following the semiclassical theory of Fermann and Auerbach [25] was presented. When applied to pure Fe, good agreement was obtained with experimental data.

The H diffusion coefficient in $Fe_{15}Cr$, as predicted through a random walk model in a lattice with blocked sites, showed a modest reduction of ~10% with respect to pure Fe.

The present results suggest that the predicted permeation coefficient of H in $Fe_{15}C$ is significantly lower than that of pure iron mainly due to solubility effects; the reduction factor is highly compatible with experimental data of materials with similar composition.

Acknowledgements

This work received financial support from the Agencia Nacional de Promoción Científica y Tecnológica, Argentina, project PICT-2014-2170. Calculations were mainly performed in the Isaac Cluster, Comisión Nacional de Energía Atómica, Argentina.

Appendix A. Supplementary material

Supplementary data associated with this article can be found, in the online version, at https://doi.org/10.1016/j.commatsci.2018.07.066.

References

[1] R.L. Klueh, A.T. Nelson, Ferritic/martensitic steels for next-generation reactors, J. Nucl. Mater. 371 (2007) 37–52.
[2] R.K. Dayal, N. Parvathavarthini, Hydrogen embrittlement in power plant steels, Sadhana 28 (2003) 431–451.
[3] C. Hurtado-Noreña, C.A. Danón, M.I. Luppo, P. Bruzzoni, Evolution of minor phases in a 9PctCr steel: effect of tempering temperature and relation with hydrogen trapping, Metall. Mater. Trans. A 46 (2015) 3972–3988.
[4] R.A. Oriani, The diffusion and trapping of hydrogen in steel, Acta Metallurgica 18 (1970) 147–157.
[5] C. Hurtado-Noreña, P. Bruzzoni, Effect of microstructure on hydrogen diffusion and trapping in a modified 9%Cr–1%Mo steel, Mater. Sci. Eng. A 527 (2010) 410–416.
[6] C. Gesnouin, A. Hazarabedian, P. Bruzzoni, J. Ovejero-García, P. Bilmes, C. Llorente, Effect of post-weld heat treatment on the microstructure and hydrogen permeation of 13CrNiMo steels, Corros. Sci. 46 (2004) 1633–1647.
[7] J. Xu, X.Z. Yuan, X.K. Sun, B.M. Wei, Hydrogen permeation and diffusion in a 0.2C-13Cr martensitic stainless steel, Scripta Metallurgica et Materialia 28 (1993) 925–930.
[8] E. Riecke, Untersuchungen zum Einfluß des Stahlgefüges auf die stationäre Wasserstoffpermeation, Werkstoffe und Korrosion 32 (1981) 66–72.
[9] A.D. Le Claire, Permeation of gases through solids, Diffusion Defect Data 33 (1983) 1–66.
[10] E. Riecke, K. Bohnenkamp, Über den Einfluß von Gitterstörstellen in Eisen auf die Wasserstoffdiffusion, Zeitschrift für Metallkunde 75 (1984) 76–81.
[11] W.A. Counts, C. Wolverton, R. Gibala, First-principles energetics of hydrogen traps in α-Fe: point defects, Acta Materialia 58 (2010) 4730–4741.
[12] D.A. Mirzaev, A.A. Mirzoev, K.Yu. Okisheva, M.S. Rakitin, Theory of hydrogen solubility in binary iron alloys based on ab initio calculation results, Mol. Phys. 110 (2012) 1299–1304.
[13] V.P. Ramunni, C. Hurtado-Noreña, P. Bruzzoni, Ab-initio approach to study hydrogen diffusion in 9Cr steels, Phys. B: Condens. Matter 407 (2012) 3301–3304.
[14] D.E. Jiang, E.A. Carter, Diffusion of interstitial hydrogen into and through bcc Fe from first principles, Phys. Rev. B 70 (2004) 064102.
[15] I. Mirebeau, M. Hennion, G. Parette, First measurement of short-range-order inversion as a function of concentration in a transition alloy, Phys. Rev. Lett. 53 (1984) 687–690.

[16] G. Bonny, D. Terentyiev, L. Malerba, On the α-α' miscibility gap of Fe-Cr alloys, Scripta Materialia 59 (2008) 1193–1196.
[17] G. Kresse, J. Furthmüller, Efficient iterative schemes for ab initio total-energy calculations using a plane-wave basis set, Phys. Rev. B 54 (1996) 11169.
[18] G. Kresse, D. Joubert, From ultrasoft pseudopotentials to the projector augmented-wave method, Phys. Rev. B 59 (1999) 1758.
[19] P.E. Blöchl, O. Jepsen, O.K. Andersen, Improved tetrahedron method for Brillouin-zone integrations, Phys. Rev. B 49 (1994) 16223.
[20] C. Varvenne, F. Bruneval, M. Marinica, E. Clouet, Point defect modeling in materials: coupling ab initio and elasticity approaches, Phys. Rev. B 88 (2013) 134102.
[21] R.C. Pasianot, On the determination of defect dipoles from atomistic simulations using periodic boundary conditions, Philos. Mag. Lett. 96 (2016) 447–453.
[22] V.P. Ramunni, R.C. Pasianot, P. Bruzzoni, Search of hydrogen transition states on Fe (bcc): the monomer adapted to first principles calculations, Phys. B – Conden. Matter 404 (2009) 2880–2882.
[23] K.W. Kehr, Hydrogen in Metals I, Springer, Berlin, 1978, p. 197.
[24] D. Sholl, J.A. Steckel, Density Functional Theory: A Practical Introduction, Wiley, 2009 p. 158 ff.
[25] J.T. Fermann, S. Auerbach, Modeling proton mobility in acidic zeolite clusters. II. Room temperature tunneling effects from semiclassical rate theory, J. Chem. Phys. 112 (2000) 6787–6794.
[26] G.H. Vineyard, Frequency factors and isotope effects in solid state rate processes, J. Phys. Chem. Solids 3 (1957) 121–127.
[27] N.R. Quick, H.H. Johnson, Hydrogen and deuterium in iron, 49–506 °C, Acta Metallurgica 26 (1978) 903–907.
[28] G. Benamati, E. Serra, Hydrogen behaviour in the aged low activation martensitic steel F82H for fusion reactor applications, Report ENEA RT/ERG/FUS/97/6 (1997) – IT9800384; Mater. Sci. Technol. 14 (1998). pp. 573–578.
[29] H. Zhou, Y. Hirooka, N. Ashikawa, T. Muroga, A. Sagara, Gas- and plasma-driven hydrogen permeation through a reduced activation ferritic steel alloy F82H, J. Nucl. Mater. 455 (2014) 470–474.
[30] I. Peñalva, G. Alberro, J. Aranburu, F. Legarda, J. Sancho, R. Vila, C.J. Ortiz, Influence of the Cr content on the permeation of hydrogen in Fe alloys, J. Nucl. Mater. 442 (2013) S719–S722.
[31] C. Hurtado-Noreña, Ph. D Thesis, Instituto Sabato, Comisión Nacional de Energía Atómica-Universidad de General San Martín, Argentina, 2010.
[32] J.L. Mijares, C. Hurtado-Noreña, P. Bruzzoni, Centro Atómico Constituyentes, Comisión Nacional de Energía Atómica, Argentina. Unpublished work.
[33] E. Riecke, B. Johnen, H.J. Grabke, Effects of alloying elements on the corrosion and hydrogen uptake of iron in sulfuric acid. Part I: permeation, diffusion and solubility of hydrogen in binary iron alloys, Werkstoffe und Korrosion 36 (1985) 435–441.
[34] W. Schwarz, H. Zitter, Löslichkeit und Diffusion von Wasserstoff in Eisenlegierungen, Archiv fur das Eisenhuttenwesen 36 (1965) 343–349.
[35] D.M. Coldwell, R.B. McLellan, Thermodynamic properties of Fe-Cr-H ternary solid solutions, Acta Metallurgica 23 (1975) 57–61.